Available online at www.sciencedirect.com
SCIENCE DIRECT®
ELSEVIER
Journal of Solid State Chemistry 179 (2006) 2271–2280
JOURNAL OF SOLID STATE CHEMISTRY
www.elsevier.com/locate/jssc

Fabrication of MnAs microstructures on GaAs(0 0 1) substrates and their electrical properties

Y. Takagaki*, E. Wiebicke, L. Däweritz, K.H. Ploog

Paul-Drude-Institut für Festkörperelektronik, Hausvogteiplatz 5-7, 10117 Berlin, Germany

Received 19 December 2005; received in revised form 29 January 2006; accepted 5 February 2006
Available online 13 March 2006

Dedicated to the occasion of the 75th birthday of Prof. Hans Georg von Schnering

Abstract

We explore wet and dry etching processes of thin MnAs layers grown on GaAs(0 0 1) substrates for microstructuring. Most of the common wet chemical etch solutions for GaAs react with MnAs strongly and in a peculiar manner. Unidirectional cracks are generated when the MnAs layers are thicker than 100 nm. We demonstrate that the crack generation can be avoided by choosing a suitable etch solution or etch temperature. We fabricate submicrometer-wide MnAs wires using Ar ion milling. The resistivity of the narrow channels is measured over a temperature range covering the phase transitions in MnAs between the α, β, and γ phases. The resistivity along the MnAs[0 0 0 1] direction is found to be smaller than that along the MnAs[1 1 $\bar{2}$ 0] direction regardless of the phase. A nearly linear temperature variation of the phase fraction is deduced in the α–β phase coexistence regime. The temperature coefficients of the resistivities are negative for the nonmagnetic phases.
© 2006 Elsevier Inc. All rights reserved.

PACS: 75.50.−y; 62.20.Mk; 72.15.−v

Keywords: Manganese arsenide; Wet chemical etching; Microstructure; Resistivity

1. Introduction

In devices whose operation is based on the manipulation of the spin instead of, or in addition to, the electron charge, injecting and detecting spin currents play an essential role. A straightforward way to accomplish these tasks is attaching ferromagnets to nonmagnetic conducting channels. MnAs is one of the prospective materials for constructing such device elements as it is ferromagnetic at room temperature and can be grown epitaxially on GaAs [1]. The latter is advantageous since ferromagnetic components can be integrated into the electrical and/or optical devices prepared in GaAs with nearly perfect interfacial properties.

MnAs is attractive also for magnetic storage devices. Since the 1950s, the data storage density has increased steadily at a rate of one order of magnitude in six years [2,3]. In near future, the size of the storage cells is expected to enter the regime of superparamagnetism. Ferromagnetic particles cannot hold their magnetization when the anisotropy in the magnetic energy, which is in proportion to the volume of the particles, is small compared to the thermal energy k_BT. The thermal instability thus imposes a limit on the storage density. The relaxation of the magnetization in small MnAs dots was demonstrated to be slow owing to the large uniaxial magnetocrystalline anisotropy [4]. In spite of the benefits of stabilizing the magnetization, the uniaxial anisotropy cannot be made too large in practice as the external magnetic field for recording magnetic data scales in proportion to the strength of the anisotropy. While the magnetization can be kept rigid at room temperature down to considerably small sizes, the coercivity of MnAs diminishes at the Curie temperature $T_c \approx 40\,^{\circ}$C. The material is, therefore, ideal for thermally assisted magnetic recording [5], which is a scheme performing the recording at an elevated temperature to reduce the coercivity. Moreover,

*Corresponding author. Fax: +49 30 2037 7515.
E-mail address: takagaki@pdi-berlin.de (Y. Takagaki).

0022-4596/$ - see front matter © 2006 Elsevier Inc. All rights reserved.
doi:10.1016/j.jssc.2006.02.008

MnAs has a unique magnetic property which is ideal for this application, i.e., the ferromagnetism in MnAs is lost discontinuously [6]. The magnetization is, therefore, unusually large even for temperatures just below T_c, and the magnetic anisotropy can be substantial to prevent the thermal randomization.

In fabricating these so-called spintronic devices or recording elements, processing MnAs layers turns out rather cumbersome due to the remarkable chemical reactivity of Mn [7,8]. In this paper, we investigate various features which MnAs layers develop when they are subject to etching. The generation of unidirectional cracks during wet chemical etching using ordinary etch solutions, if the layer thickness is larger than a critical value, is probably the most problematic phenomenon. We demonstrate methods to avoid the crack generation. With respect to dry etching, MnAs is highly resistive to reactive ions. Ar ion milling appears to be the only possibility so far, except under special circumstances [8], to fabricate submicrometer channels. We examine the electrical properties of the thus defined narrow channels in the temperature regime where MnAs transforms itself between the α, β, and γ phases.

2. Epitaxial MnAs layers on GaAs

We employ in our investigations MnAs layers grown on GaAs substrates by molecular beam epitaxy (MBE). A number of crystal orientations of the MnAs layers can be realized by choosing appropriate surface orientations of the substrates and optimizing the growth conditions [9–12]. Throughout this paper, the surface planes of the MnAs layers and the GaAs substrates are set to be $(\bar{1}\,1\,0\,0)$- and $(0\,0\,1)$-oriented, respectively. The growth temperature was $230-250\,^{\circ}$C under an As_4/Mn beam equivalent pressure ratio of 70 [13]. The epitaxial orientation relationship is such that the $[0\,0\,0\,1]$ and $[1\,1\,\bar{2}\,0]$ directions of MnAs are parallel to the $[1\,\bar{1}\,0]$ and $[1\,1\,0]$ directions of GaAs, respectively. Bulk MnAs possesses a strong uniaxial magnetocrystalline anisotropy with the magnetic hard axis along the $[0\,0\,0\,1]$ direction. While the $(0\,0\,0\,1)$ plane is the magnetic easy plane, the magnetic moments in the epitaxial thin films are oriented along the $[1\,1\,\bar{2}\,0]$ direction due to the shape anisotropy.

Two phase transitions occur in bulk MnAs between the above-mentioned growth temperature and room temperature. The low-temperature phase, α-MnAs, is ferromagnetic and has a hexagonal crystal structure. A first-order phase transition takes place at about $40\,^{\circ}$C. At $126\,^{\circ}$C, MnAs undergoes a second-order phase transition. The medium-temperature phase, β-MnAs, loses the ferromagnetism and the crystal structure transforms to be orthorhombic. The phase during the epitaxial growth is the γ phase, which is paramagnetic and the crystal structure is hexagonal. A bulk MnAs crystal exhibits inherent characteristics of a first-order phase transition at $T_c \approx 40\,^{\circ}$C, i.e., an abrupt transition and a thermal hysteresis (about $10\,^{\circ}$C). However, this is no longer the case for epitaxial thin layers. The α and β phases coexist over a wide temperature range around T_c [14]. As we show below, the wet chemical etching of MnAs is profoundly influenced by the simultaneous presence of the two phases.

The phase coexistence originates from the stress evolution in MnAs/GaAs heterostructures [14]. During the MBE growth, MnAs layers are nearly free of the stress as misfit dislocations are incorporated at the MnAs/GaAs interface. The difference in the lattice constants between MnAs and GaAs can thus be disregarded. In cooling the sample from the growth temperature, the thermal expansion mismatch results in tensile strain in the MnAs layers. A crucial fact is that the thermal expansion coefficient of MnAs is significantly large, $5.8 \times 10^{-5}/^{\circ}$C for the β phase [15] and $2 \times 10^{-5}/^{\circ}$C for the γ phase [16]. In comparison, the thermal expansion coefficient of GaAs is $5.9 \times 10^{-6}/^{\circ}$C. The accumulation of the thermal stress continues steadily with decreasing the temperature down to T_c. When the first-order phase transition sets in, however, the stress suddenly reverses its sign. The phase transition between the α and β phases involves a discontinuous volume change due to magnetostriction, i.e., α-MnAs is 1.9% larger than β-MnAs. Correspondingly, the stress in the MnAs layers imposed by the substrate changes to be compressive when the temperature is lowered beyond T_c. (The abrupt lattice expansion/contraction is so huge that bulk MnAs crystals were observed to generate microcracks after thermal cycles [17,18].) The simultaneous existence of both of the phases is energetically favored as the thermal and phase-transition stresses are compensated with each other [19]. The temperature range for the coexistence shifts according to the relative strength of the two stresses. The range extends to the high- or low-temperature side of T_c if the thermal or phase-transition stress is dominant, respectively.

The distribution of the two phase-domains depends on the orientation of the c-axis of MnAs with respect to the surface plane. The sudden volume change at the phase transition takes place in the directions normal to the c-axis. The lattice constant along the c-axis is almost identical between the α and β phases. The anisotropic change of the lattice constants gives rise to a periodic repetition of α- and β-MnAs in the MnAs$[1\,1\,\bar{2}\,0]$ direction with submicron-scale periods in MnAs$(\bar{1}\,1\,0\,0)$/GaAs$(0\,0\,1)$ heterostructures. The period d increases almost linearly with the film thickness t as $d \approx 4.8t$ [20]. As we see below, the wet chemical etching of MnAs layers suffers from the fact that the stress retains the full strength in the MnAs$[0\,0\,0\,1]$ direction, as there exists no stress reduction mechanism in that direction. We note that the shape of the phase domains possesses a quasi-sixfold symmetry when the substrates are GaAs$(1\,1\,1)$B, for which MnAs is $(0\,0\,0\,1)$-oriented. Submicrometer-size islands of α-MnAs are interwoven in a honeycomb-like network of β-MnAs [21]. The etching characteristics of the MnAs$(0\,0\,0\,1)$/GaAs$(1\,1\,1)$B heterostructures are qualitatively similar to those of MnAs$(\bar{1}\,1\,0\,0)$/GaAs$(0\,0\,1)$ heterostructures.

3. Wet chemical etching of MnAs layers on GaAs

3.1. Peculiar etching behavior

Although MnAs is listed in [22] as soluble in HCl, we have encountered that etching of our MBE-grown MnAs layers is not possible using HCl, unless H_2O_2 is added [23,24]. To the extent we have investigated so far, all the etch solutions for GaAs remove MnAs efficiently. However, the etching progresses in a peculiar fashion for acidic solutions. In Fig. 1, we show scanning-electron-microscopy (SEM) images of the MnAs surface when the etching using a $HCl : H_2O_2 : H_2O = 5 : 1 : 50$ solution at 25 °C was discontinued during the removal of a MnAs layer (140 nm thick). Similar surface features were observed when HCl was replaced by H_2SO_4. The MnAs layer was etched through a square-shaped window defined in a resist. The SEM images were taken from the area around a corner of the etch window after the resist had been stripped off. Fig. 1(a) shows the surface shortly after the initiation of the etching, whereas in Fig. 1(b) the MnAs layer was mostly removed. The partially etched MnAs layers reveal the following characteristics: (i) the epitaxial layer develops unidirectional cracks which are distanced with fairly regular intervals [8]. The cracks always run in the MnAs[$1 1 \bar{2} 0$] direction. (ii) Stripe patterns show up in the MnAs strips sandwiched by the cracks. They are clearly visible in Fig. 2 as a step-like height modulation in the MnAs-side of the etch border. The stripes and the cracks are orthogonal to each other. (iii) The surface exhibits a porous appearance, in particular, in the deep segments of the surface corrugation.

The porosity is closely associated with a severe alteration of the surface stoichiometry by the etching. Energy dispersive X-ray (EDX) spectrometry and Raman scattering measurements indicate that the porous substance is nothing but amorphous As [7]. That is, Mn species are almost instantaneously extracted from the MnAs layer and a pile of amorphous As is left on the GaAs substrate. The porous parts of the layer are thus nonconductive. It is immediately apparent that the etching is not the kind that allows us to vary the thickness of the MnAs layers by controlling the etching time.

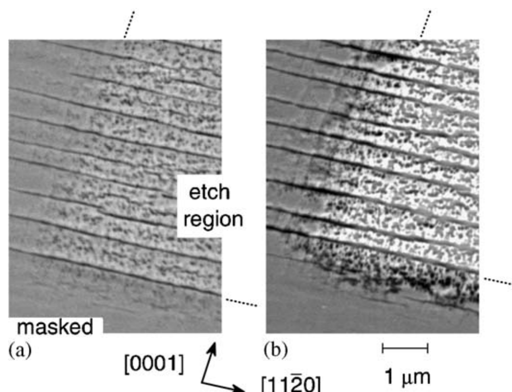

Fig. 1. Scanning electron micrographs of MnAs surface during wet chemical etching using a $HCl/H_2O_2/H_2O$ solution at room temperature. The thickness of the MnAs layer is 140 nm. The dotted lines indicate the border of the etch window defined by a resist. The crystal directions of MnAs are indicated by the arrows.

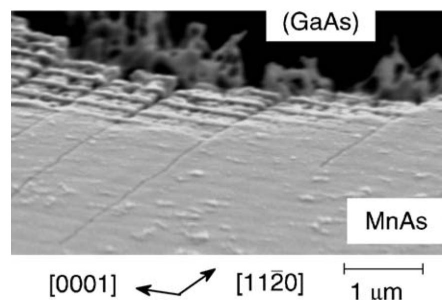

Fig. 2. Glancing angle view of the surface of a partly etched MnAs film grown on a GaAs(0 0 1) substrate. The thickness of the MnAs layer is 140 nm. Following wet chemical etching using a $HCl/H_2O_2/H_2O$ solution at room temperature and the removal of the resist, the sample was etched using Cl_2 reactive ion etching. The dry etching etched the GaAs substrate 5 μm deep in the etch window region indicated as "(GaAs)". The crystal directions of MnAs are indicated by the arrows.

The generation of the cracks is a manifestation of the large stress accumulated in the MnAs layers. As the wet etching proceeds in the above-mentioned unusual style, the stress cannot be accommodated in the MnAs layers. The resulting breakdown of the stress balance is responsible for the layers breaking into pieces. While the α–β coexistence nearly nullifies the stress in the MnAs[$1 1 \bar{2} 0$] direction, the thermal expansion stress remains intact in the MnAs[0 0 0 1] direction. For this reason, the cracks are unidirectional and run always perpendicular to the c-axis of MnAs. It is noteworthy that as-grown layers crack during the cooling procedure following the growth if the layer thickness exceeds about 0.5 μm [13]. These cracks appear also as parallel lines stretched along the MnAs[$1 1 \bar{2} 0$] direction. For MnAs layers thinner than about 100 nm, the cracks are no longer generated even during the etching as the accumulated stress is not sufficiently strong [8]. The SEM image in Fig. 3(a) shows the partially etched surface of a 90-nm-thick MnAs film. Although the porosity is still present, the cracks are absent.

The narrow MnAs strips, which are produced as a consequence of the unidirectional cracks, develop a corrugation-like feature in the length direction. The evolution of this feature in the course of the etching is conveniently displayed in Fig. 2. We call our attention to the fact that the remaining MnAs layer here, which was covered by a resist, was unintentionally etched due to underetching in the lateral direction. The etch time is hence longer for the areas closer to the etch window, which is indicated as "(GaAs)". The α–β stripe structure in as-grown MnAs/GaAs(0 0 1) heterostructures is accompanied by a similar height modulation resulting from the different lattice constants of α- and β-MnAs [14]. The segments of the α and β phases correspond to the ridges and grooves,

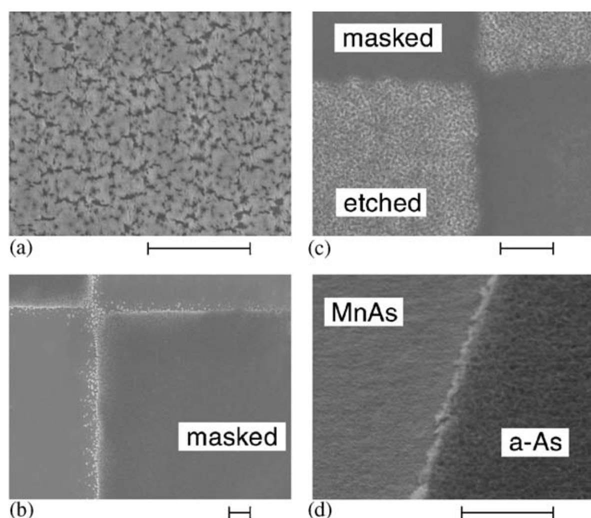

Fig. 3. Scanning electron micrographs of MnAs surfaces after various wet chemical etching processes. A MnAs layer with an initial thickness of 90 nm was etched in (a) using a $HCl/H_2O_2/H_2O$ solution at 23 °C. A MnAs layer with an initial thickness of 130 nm was etched in (b) using the same solution at 60 °C. The 130-nm-thick MnAs layer was etched using a $KOH/H_2O_2/H_2O$ solution at 23 °C for 45 s in (c) and for 30 s in (d). In (d) the surface amorphous As layer, which is visible on the right-hand side indicated as "a-As", has detached from the surface during the etching, revealing the underlying MnAs layer seen on the left-hand side. The image in (d) was taken from a glancing angle to enhance the contrast associated with the surface roughness. The scale bars indicate the length of 1 μm.

respectively. The magnitude of this modulation is, however, only a few nm and is too small to be visible in SEM. The corrugations in Figs. 1 and 2 have much larger amplitudes and, in fact, result from the enormously different etch rates for α- and β-MnAs. By identifying the distribution of α- and β-MnAs using magnetic force microscopy (MFM), we have established that α-MnAs is etched faster than β-MnAs [8,25,26]. The segments of β-MnAs thus form the ridges. Notice that the phase composition associated with the corrugation due to the etching is the other way around in comparison to the tiny height modulation prior to the etching resulting from the α–β stripes.

3.2. Avoiding crack generation

The peculiar features in the wet chemical etching described in the preceding subsection are problematic in processing MnAs layers to microstructures. The cracking of the layers is particularly a serious issue as the cracks extend far into the resist-covered region [8,25], i.e., the influences of the etching are not restricted within the etched region. Moreover, as the etch solutions are poured into the mask-protected regions through the cracks, the border between the etched and masked regions becomes considerably obscure and underetching occurs on a massive scale, in particular, in the MnAs$[1 1 \bar{2} 0]$ direction, see Fig. 1. Preventing the crack generation is, therefore, of particular importance in fabricating microstructures. We demonstrate below two methods to fulfill the requirement.

The first possibility is carrying out the etching at high temperatures. It was observed in [25] that the cracks were absent in the etched surface when the layer was composed entirely of the β phase at temperatures $T > 60\,°C$. The critical temperature for the disappearance of the crack generation coincides with the upper onset of the phase coexistence irrespective of the layer thickness [25]. This implies that the thermal stress alone does not cause the cracks during etching, plausibly because the layer thickness is much smaller than the critical thickness for the crack generation in as-grown layers. Instead, vertical components of the stress resulting from the uneven surface that evolves during the etching in the temperature regime of the phase coexistence are suggested to trigger the crack generation. Interestingly, MnAs layers crack with even stronger forces than at room temperature when the layers are etched at low temperatures, where MnAs is entirely of the α phase [25]. The thermal expansion coefficient of α-MnAs is negative, $-1.0 \times 10^{-4}/°C$ [15]. The compressive stress in α-MnAs layers thus further increases with decreasing temperature. The gigantic compressive stress is expected to be the driving force of the cracking in this regime.

In Fig. 3(b), we show a surface image when the etching was performed at 60 °C under the condition that no domains of α-MnAs exist. The surface features are similar to those in Fig. 3(a), i.e., when the thickness of MnAs layers is smaller than the critical value. In spite of the complete removal of the MnAs layer in the etched region, no extensive cracks are found in the resist-covered MnAs regions. (Microcracks having a length of several hundred nm are occasionally observed if the etch temperature is only slightly above the coexistence temperature regime.) Nevertheless, the porosity at the boundary of the masked segments indicates that the underetching takes place again in the form of massive extraction of Mn species. Another disadvantage of this high-temperature wet etching method is the difficulty in controlling the etch rate. The etch rate is seriously affected by the evaporation of H_2O_2. We point out, however, that a "shallow etching technique" can be adopted if the purpose of the etching is to define conducting channels. The MnAs layers are no longer conductive once Mn species are extracted, and so the "etch depth" needs not be controlled precisely in this case.

As the presence of the α–β stripes appears to be a critical factor in the generation of the cracks when the layers are etched at room temperature, the crack generation might be avoided by a certain surface treatment that prevents the formation of the α–β stripes. To test the idea, we carried out an etching with a bombardment of the MnAs layers by Ar or N_2 ions prior to the etching. The acceleration voltage was 0.7 kV or below. Although some indications of the reduction of the number of cracks were found, the attempts were unsuccessful as the crystal damages were limited to the very surface of the MnAs layer for the applied ion energy.

The second possibility is to use alkaline etch solutions. In Figs. 3(c) and (d), we show the surface images when an aqueous alkali solution ($KOH : H_2O_2 : H_2O = 1 : 1 : 150$) was used. We found absolutely no cracks in the SEM observations of the etched surface. In addition to the absence of the cracks, we have found that the partly etched MnAs layer remarkably remains conductive. The alkaline etching is hence promising if thinning the layers by way of a "layer-by-layer" removal of the material is required. The etching still appears to progress by removing Mn species from the epitaxial layer as we observe a rugged surface layer, plausibly consisting of amorphous As, on the etched surface as shown in Fig. 3(c). However, the boundary between the amorphous As surface layer and the underlying MnAs layer is abrupt. The amorphous As surface layer is sometimes detached from the surface during the etching, leaving a specular surface of MnAs as shown on the left-hand side of Fig. 3(d). In Fig. 4, we plot the dependence of the two-terminal conductance of a 130-nm-thick MnAs film on the etch time. A nearly linear decrease of the conductance, which is proportional to the thickness of the MnAs layer, with the etch time is found, evidencing the presence of a well-defined etch front. The etch rate estimated from the slope is 2.5 nm/s. We have also examined the wet chemical etching of MnAs films using KOH-based etch solutions having pH values ranging from 8 to 13. The etching characteristics remained similar, apart from the smaller etch rate for larger pH values.

The practically conventional way of the etching is probably realized by the weak solubility of Mn in KOH-based etch solutions. In Fig. 5, we show the Pourbaix diagram for Mn. We indicate also the oxidation–reduction potential E of aqueous-KOH and acidic solutions by the thick solid and dashed lines, respectively [27,28]. One finds that manganese is deposited as oxides in KOH-based etch solutions. In acid-based solutions, on the contrary, manganese is stable as Mn^{2+} ion, and hence dissolves in the solutions. It is noteworthy that a contact of MnAs layers with water often leaves a sign of some reaction on the MnAs surface. Manganese is seen to be also stable as the soluble Mn^{2+} ion at $pH = 7$ provided that $0.1\,V > E > -1.1\,V$. Although $E \approx 0.7\,V$ for ultrapure water, E can be as low as $-0.3\,V$ if the water contains less O_3 and more H_2 [27,28].

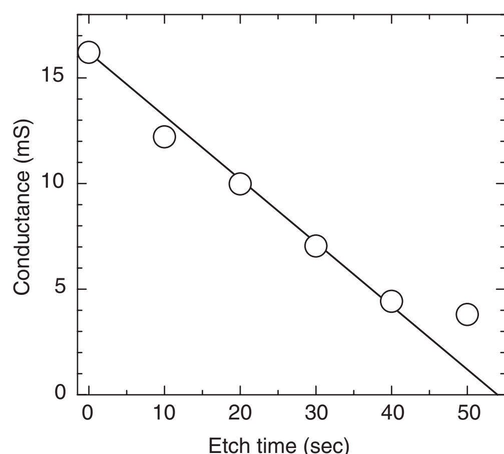

Fig. 4. Variation of the two-terminal conductance of a MnAs layer when the layer is etched using a $KOH : H_2O_2 : H_2O = 1 : 1 : 150$ solution. The initial layer thickness is 130 nm. The samples are 4.5 mm long and 1.0 mm wide. The etch rate estimated from the slope shown by the solid line is 2.5 nm/s.

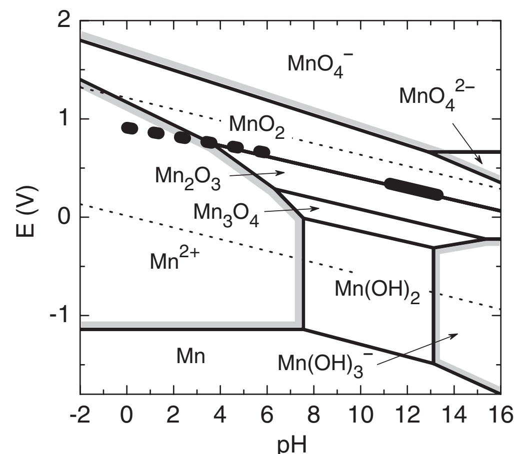

Fig. 5. Pourbaix diagram for manganese at 25 °C. The oxidation–reduction potential E of acidic (HCl, H_2SO_4, and HNO_3) and aqueous alkali (KOH) solutions [25,26] is indicated by the thick dotted ($0 < pH < 6$) and solid ($11 < pH < 13$) lines, respectively.

3.3. Spontaneous microcrystal growth

Under a circumstance that a large amount of amorphous As covers the GaAs substrate, micrometer-size crystals have been observed to grow spontaneously in a time scale of a few days [7]. Some examples of the microcrystals are shown in Fig. 6. The microcrystals appear in various shapes, including pyramidal, cubic, hexagonal, and whisker-like ones. The size distribution of the microcrystals is rather large. The typical size is a few μm. However, the crystals can be as large as 10 μm.

The microcrystals were evidenced by EDX to consist of arsenic and oxygen. A possible inclusion of manganese was ruled out within the detection limit of EDX. Raman scattering spectra exhibited sharp peaks originating from the microcrystals [7]. The peaks are associated with a cubic crystalline form of arsenic oxide (As_2O_3), known as arsenolite. Arsenolite crystals sublime at 193 °C. The microcrystals are indeed annihilated by heating the samples to such a temperature.

The microcrystals were observed not to grow as long as the etched sample was kept in vacuum [7], indicating that they are formed by the oxidation of the amorphous As layer. The rapid oxidation and crystallization are driven by the Mn species extracted during the etching. The hydrogen peroxide in the etch solution oxidizes the manganese in the MnAs layer to MnO_2, which is a catalyst for oxidation.

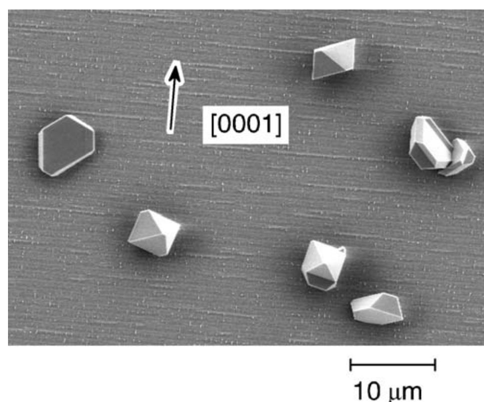

Fig. 6. Scanning electron micrograph of spontaneously grown microcrystals. A layer of amorphous As is left on the GaAs substrate from a wet-chemically etched MnAs layer. The direction of the *c*-axis of MnAs is indicated by the arrow. The microcrystals consist of the cubic crystalline form of As_2O_3 (arsenolite).

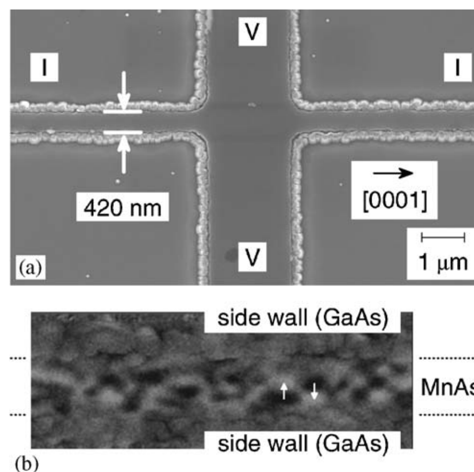

Fig. 7. (a) Scanning electron micrograph of MnAs narrow channels fabricated by using Ar ion milling. The width of the narrow channel, which is marked by "I", is 0.42 μm. Voltage leads, which are indicated as "V", having a width of 2 μm are attached to this channel by forming an asymmetric cross junction. (b) Magnetic force micrograph of the narrow horizontal channel. The MnAs channel and GaAs side-wall segments are indicated. The image was taken from a 3-μm-long portion of the channel. The vertical arrows indicate an example of in-plane magnetic moments in the magnetic domain structure.

Although MnO_2 is also known to be a very effective oxidant of As(III) to As(V) [29], we believe that the spontaneous oxide growth is caused by a catalytic reaction as the microcrystals do not grow in a vacuum environment. The microcrystals grow also on the surface of as-grown MnAs layers. However, the spontaneous growth in this case takes place on much longer time scales, since MnO_2 has to be produced first by a natural oxidation of manganese. In the case of the wet chemical etching, the spontaneous growth takes place only during the first several days after an etching even if a large amount of amorphous As is still left on the surface. We speculate that MnO_2 is completely surrounded by As_2O_3, and so the rapid oxidation ceases to occur as all the catalytic species are isolated from the amorphous As.

4. Dry etching of MnAs layers

4.1. Fabrication of MnAs narrow channels

Our attempts to etch MnAs layers using reactive ion etching (RIE) have not been successful so far. The etch rate using Cl_2 gas is virtually zero. The image in Fig. 2 was taken, in fact, from a sample on which Cl_2 RIE was carried out after stripping the resist following a wet chemical etching. (The GaAs region was etched 5 μm deep and hence appears as the black area on the top side of the image.) The MnAs region is unaffected by the RIE, except removing amorphous As in the partially etched area, thereby highlighting the step-like height modulation. Ar ion milling, therefore, appears to be the only method to fabricate nanometer-scale structures from MnAs films. It should be noted, however, that the thickness of the MnAs layers that can be processed by ion milling to submicron structures is practically limited to be smaller than about 100 nm due to the low etch rate.

In Fig. 7(a), we show a SEM image of the cross-junction portion of a narrow-channel Hall-bar structure fabricated using Ar ion milling. The width of the channel, which is marked by "I", is 0.42 μm. The voltage probes, which are marked by "V", are 2.0 μm wide. These channels have a remarkably uniform width. The absence of geometrical defects throughout the narrow channels longer than 500 μm was confirmed by resistance measurements.

The fabrication procedure of the submicron channels is illustrated in Fig. 8. An important feature of our process is that a metal mask for the ion milling is not deposited directly on the MnAs layer. This is because the etch solution for the metal removal is likely to react with MnAs, at least, to a certain extent. To begin with, we prepare a composite system consisting of negative-resist, Ti metal, and polymetyl-methacrylate (PMMA) layers on the surface of a MnAs layer, Fig. 8(a). The Hall-bar pattern is defined by exposing the double layers of the negative resist (XAR-N 7520/18, Allresist, Germany) by means of electron beam lithography. On developing the resist, a Ti mask pattern is obtained by the self-aligned lift-off technique, Fig. 8(b). The PMMA layer outside the mask is then removed using O_2 plasma etching, Fig. 8(c). The MnAs layer is finally etched using Ar ion milling at an acceleration voltage of 270 V, Fig. 8(d). We used an r.f. power of 75 W. The pressure in the RIE chamber was 1 Pa with a flow rate of Ar gas of 10 sccm. The sputtering rate of MnAs was 2.5 nm/min. The purpose of inserting the PMMA layer in this process is twofold. First, the developer for the negative resist is alkaline and thus reacts with MnAs. The PMMA layer protects the MnAs layer from this reaction. Second, the negative resist is hardened by the Ar sputtering and is often difficult to remove after the processing. The PMMA layer is used here as a

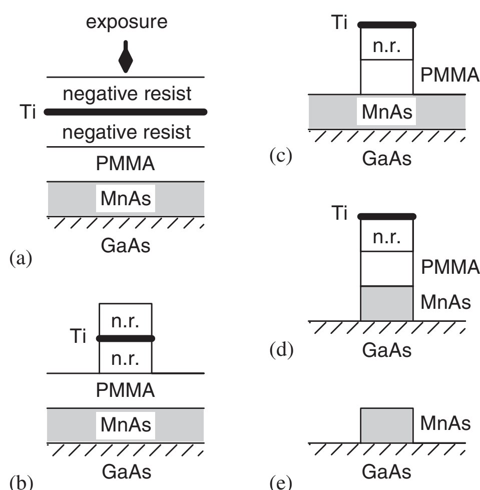

Fig. 8. Fabrication procedure of MnAs microstructures. The process consists of (a) electron beam lithography, (b) self-aligned lift-off of Ti pattern (development of the negative resist), (c) O_2 plasma etching of PMMA, (d) Ar ion milling of MnAs, and (e) removal of the mask.

mask-release layer after the dry etching, Fig. 8(e). We note that PMMA may not be the optimum choice of the material as sputter-hardened PMMA is sometimes left as standing walls on top of the edges of the channel at the completion of the process. The PMMA layer may be replaced by a layer of other materials if they can better serve these purposes.

4.2. Magnetic properties of MnAs narrow channels

Process-induced damages are a well-known disadvantage of using Ar ion milling. To evaluate the possible influences of the damages, we have examined the magnetic properties of the MnAs channels using MFM. Fig. 7(b) shows an MFM image of the horizontal narrow channel of the Hall-bar junction in Fig. 7(a). Here, the MFM tip detected the vertical component of magnetic fields. The white and black regions correspond to the areas where the magnetic fields were directed out of and towards the surface plane, respectively. A clear magnetic contrast associated with the magnetic domain structures in the MnAs segment is visible. The magnetic properties in the initial MnAs films are hence indicated to be preserved by the microstructuring. For typical ferromagnetic materials, the magnetic moments in narrow wires are re-oriented along the wire direction due to the shape anisotropy. However, the magnetic moments in MnAs wires remain to be parallel to the easy axis, which is directed to be perpendicular to the wire in Fig. 7, due to the material's large uniaxial magnetocrystalline anisotropy [8,30]. A vertically neighboring pair of black and white segments is hence identified to be due to a magnetic moment, as illustrated by the arrows in Fig. 7(b).

The width of the present wire is larger than the period of the α–β stripes. The two phases of MnAs are hence expected to coexist within the wire. The medium-contrast, i.e., gray, areas in Fig. 7(b) are, therefore, assigned to be the regions of β-MnAs. (An example of them is the area immediately above the two vertical arrows.) It is, in principle, possible that these nonmagnetic regions were produced by the process-induced damages, instead of β-MnAs associated with the stripe structure. However, we rule out this possibility based on an observation in [30] that MnAs disks having a diameter of 100 nm, which is significantly smaller than the α–β stripe period, exhibited a fully ferromagnetic appearance in MFM, i.e., the disks were entirely composed of α-MnAs. As further evidence, we point out that the fact that the crack generation in wet chemical etching could not be avoided even when the MnAs surface was intentionally damaged as we described in Section 3.2 implies that the influences of the damages induced in our fabrication procedure on the structural properties of MnAs are negligibly small.

In contrast to Ar ion milling, wet chemical etching leaves no influence on the magnetic and structural properties of MnAs as long as the border between the Mn-extracted substance and the unetched MnAs is sharply established. It was possible in [8] to define MnAs channels having a width of several hundred nm using a wet chemical etching by exploiting the etch selectivity between α- and β-MnAs. The magnetic properties were confirmed to be unaltered using MFM.

5. Electrical properties of MnAs channels

In this section, we examine the electrical properties of narrow MnAs channels fabricated using the Ar ion milling process described in the preceding section. Fig. 9 shows the temperature dependence of the resistivity in two orthogonal in-plane directions [31–35]. The direction of the current

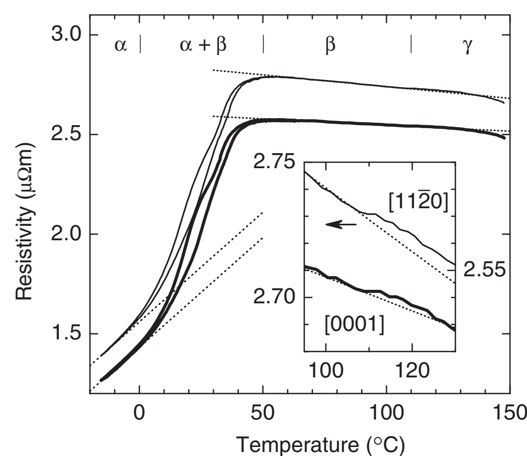

Fig. 9. Temperature dependence of the resistivities of 50-nm-thick MnAs wires on GaAs(0 0 1). MnAs channels having widths of 1.22 and 0.94 μm are defined in the [0 0 0 1] (thick solid line) and [1 1 $\bar{2}$ 0] (thin solid line) directions of MnAs, respectively. High-temperature resistivities are shown on expanded scales in the inset. The phase transitions in MnAs between the α, β, and γ phases are assigned as indicated. The dotted lines indicate extrapolated linear temperature dependencies of α- and β-MnAs in the coexistence regime.

flow for the resistance measurements is along the MnAs[0 0 0 1] and MnAs[1 1 $\bar{2}$ 0] directions for the thin and thick solid lines, respectively. The thickness of the MnAs layer is 50 nm. The distance between the probes for the voltage measurements is 530 μm. The width of the channel is 1.22 and 0.94 μm for the current flow along the [0 0 0 1] and [1 1 $\bar{2}$ 0] directions of MnAs, respectively. The channel width was chosen to be relatively wide in the present measurements so that the stress reduction in MnAs channels due to the side-wall exposure does not significantly alter the stripe structure in the α–β coexistence regime. The phase of MnAs is assigned as indicated at the top of the panel. Irrespective of the phase, the resistivity along the MnAs[0 0 0 1] direction is smaller than that along the MnAs[1 1 $\bar{2}$ 0] direction. The anisotropy is about 10% for α-MnAs and 7–8% for β- and γ-MnAs.

The resistivity curves reveal a thermal hysteresis in the temperature range of $0<T<50\,^{\circ}$C. As the resistivity change is not abrupt, this temperature range is identified to be the α–β coexistence regime [14]. In the regime of exclusively α phase ($T<0\,^{\circ}$C), the resistivity increases steeply with temperature. The strong temperature dependence is attributed to two contributions: spin-disorder scattering and phonon scattering [33].

The resistivities exhibit a linear temperature variation

$$\rho_{[0\,0\,0\,1]}(T) = 2.61[1 - 2.4\times10^{-4}\,T/^{\circ}\mathrm{C}]\,\mu\Omega\mathrm{m}, \quad (1)$$

$$\rho_{[1\,1\,\bar{2}\,0]}(T) = 2.86[1 - 4.1\times10^{-4}\,T/^{\circ}\mathrm{C}]\,\mu\Omega\mathrm{m} \quad (2)$$

when the MnAs layer is purely of the β phase ($50<T<110\,^{\circ}$C). The temperature coefficient for β-MnAs is negative, in agreement with the reports by Fischer and Pearson [31] and by Bärner [32,33]. The mechanism responsible for the negative coefficient is not clear at present. A similar decrease of the resistivity with increasing temperature is observed in metallic (Ga,Mn)As layers above T_c. Hirakawa et al. [36] have speculated that a hopping-type conduction is responsible for the anomaly, as infrared absorption spectroscopy indicated a nearly localized behavior of the conducting holes. As the carriers in MnAs are unlikely to be localized, the negative temperature coefficients in diluted (Ga,Mn)As and MnAs layers are expected to have different origins. A series of $D0_3$-type Fe_3D (D = Ga, Si, Al, etc.) ferromagnetic alloys having a partial replacement of Fe atoms with 3d transition metals has been reported to exhibit a negative temperature dependence above the Curie temperature [37–39]. A critical role of the gigantic spin disorder scattering in the ferromagnetic phase for the negative temperature coefficient [38] and a possible relation of the anomaly to the heavy-fermion phenomenon [39] were suggested. Spin fluctuations are crucial also in MnAs [33,40], as evidenced by the fact that the resistivity at the Curie temperature is about two orders of magnitude larger than the residual resistivity at $T\to0$ K [17].

An intriguing mechanism for a negative temperature coefficient is spin-density-wave antiferromagnetism, which has been observed, for example, in Cr [41] and its alloys [42]. An antiferromagnetic spin order with a period incommensurate with the ionic lattices can dramatically distort the Fermi surface. The magnetic superlattice induces magnetic superzone gaps. The gaps reduce the effective number of conduction carriers below the Néel temperature T_N, i.e., the opening up of the energy gap leaves less of the Fermi surface available for the conduction. An increase in the carrier density with temperature due to the gaps is responsible for the negative temperature coefficient of the resistivity below T_N.

Analyzing the negative temperature dependence of the resistivity of β-MnAs in terms of this mechanism, specifically whether the negative temperature coefficient originates from the carrier density or the scattering time, will be worthwhile as there is a theoretical suggestion that β-MnAs is antiferromagnetic instead of paramagnetic [43]. Although the magnetization in MnAs is lost at $T_c\approx40\,^{\circ}$C, the magnetic susceptibility follows the Curie–Weiss law only at $T>126\,^{\circ}$C [6]. Moreover, the loss of the magnetization at T_c is discontinuous, and one obtains an extrapolated Curie temperature of about 127 °C if the temperature dependence of the magnetization for $T<T_c$ is fitted by a Brillouin function [16]. These observations could be taken as evidence for an antiferromagnetic behavior of β-MnAs [44]. However, neutron scattering measurements have detected no sign of long-range magnetic order in β-MnAs [45,46]. Niranjan et al. [43] have proposed that the failure of neutron scattering to detect the long-range magnetic order of antiferromagnetism may be due to a weak exchange coupling between magnetically ordered Mn planes, i.e., an ensemble average over magnetically independent planes in macroscopic samples hinders the long-range order. The superzone gaps will prevail at the Fermi level if this explanation turns out correct, thereby giving rise to the observed negative temperature coefficient.

The temperature coefficient was reported to become positive in the temperature regime of γ-MnAs [31,33]. In our devices, on the contrary, the temperature coefficient remains negative, although the coefficient slightly approaches zero, see the inset of Fig. 9. The resistivity drops rapidly in Fig. 9 for $T>140\,^{\circ}$C. This strong temperature dependence is, however, due to the thermally activated parallel conduction in the semi-insulating GaAs substrate. In addition, MnAs in ambient atmosphere gradually oxidizes when the temperature is higher than about 120 °C. The slight oxidation of MnAs is partly responsible for the strong increase of the resistivity when decreasing the temperature, as the data of Fig. 9 were taken in the high-temperature regime while the samples were cooled down from the highest temperature.

Narrow segments of α-MnAs and β-MnAs repeat alternately in the [1 1 $\bar{2}$ 0] direction of MnAs when the

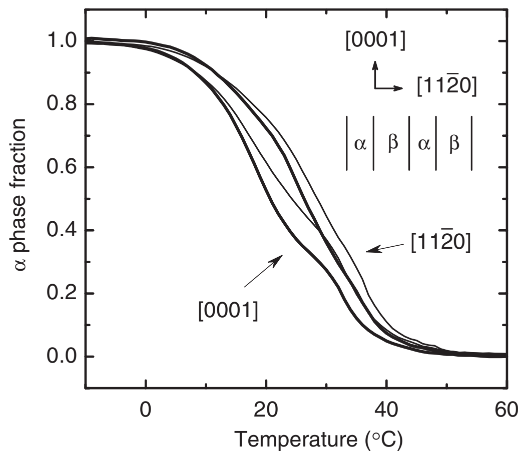

Fig. 10. Temperature dependence of the fraction of the α phase of MnAs wires on GaAs(0 0 1) derived from the resistivity data in Fig. 9. The fraction is estimated independently for the current flow along the [0 0 0 1] (thick solid line) and [1 1 $\bar{2}$ 0] (thin solid line) directions of MnAs. The inset illustrates the crystal orientations of MnAs with respect to the stripe structure formed by an alternate repetition of the α- and β-MnAs strips.

two phases coexist. The resistivities in the [0 0 0 1] and [1 1 $\bar{2}$ 0] directions are related in this case to the resistivities ρ_α and ρ_β, respectively, of the α and β phases as

$$\rho_{[0\,0\,0\,1]} = \frac{\rho_\alpha \rho_\beta}{f_\alpha \rho_\beta + (1 - f_\alpha)\rho_\alpha}, \tag{3}$$

$$\rho_{[1\,1\,\bar{2}\,0]} = f_\alpha \rho_\alpha + (1 - f_\alpha)\rho_\beta, \tag{4}$$

where f_α is the fraction of the α phase. In Fig. 10, we plot f_α deduced from the resistivity data in Fig. 9. Here, we have assumed the linear temperature dependence of the resistivities $\rho_\alpha(T)$ and $\rho_\beta(T)$ indicated by the dotted lines. Using this assumption, the ratio of the resistivities of the α and β phases at 40 °C is estimated to be about 1.4. The phase fraction is found to vary almost linearly with temperature in the coexistence range. The nearly identical results obtained independently of the direction of the current flow justify our simple model.

6. Conclusion

We have investigated the etching processes of thin MnAs layers grown on GaAs(0 0 1) substrates. The marked reactivity of manganese leads to unusual features in wet chemical etching process. An instantaneous extraction of Mn species from the MnAs layers, a generation of unidirectional cracks, and a large etch selectivity between the phases of MnAs are three prominent features. We have demonstrated that the crack generation can be avoided by using suitable alkaline etch solutions (KOH-based solutions). Carrying out wet chemical etching at high-temperatures can also significantly reduce the crack generation. Due to the outstanding durability of MnAs to reactive ions, nanometer-scale structures can be fabricated at present only using Ar ion milling. We have examined the temperature dependence and anisotropy of the resistivities of narrow MnAs channels fabricated by using the ion milling process. A nearly linear temperature variation of the phase fraction was extracted for the α–β coexistence regime. The temperature coefficient of the resistivity was negative for β-MnAs and possibly for γ-MnAs as well. Further studies of the negative temperature coefficient will provide a clue to answer the recently re-raised question concerning the magnetic state of the β-MnAs phase.

Acknowledgments

The authors would like to thank C. Herrmann for the MBE growth. Part of this work was supported by the Federal Ministry of Education and Research (nanoQUIT program).

References

[1] M. Tanaka, Semicond. Sci. Technol. 17 (2002) 327.
[2] S.H. Charap, P.-L. Lu, Y. He, IEEE Trans. Magn. 33 (1997) 978.
[3] D. Weller, A. Moser, IEEE Trans. Magn. 35 (1999) 4423.
[4] Y. Takagaki, C. Herrmann, E. Wiebicke, J. Herfort, L. Däweritz, K.H. Ploog, Appl. Phys. Lett. 88 (2006) 032504.
[5] J.J.M. Ruigrok, R. Coehoorn, S.R. Cumpson, H.W. Kesteren, J. Appl. Phys. 87 (2000) 5398.
[6] N. Menyuk, J.A. Kafalas, K. Dwight, J.B. Goodenough, Phys. Rev. 177 (1969) 942.
[7] Y. Takagaki, E. Wiebicke, M. Ramsteiner, L. Däweritz, K.H. Ploog, Appl. Phys. A 76 (2003) 837.
[8] Y. Takagaki, E. Wiebicke, T. Hesjedal, H. Kostial, C. Herrmann, L. Däweritz, K.H. Ploog, Appl. Phys. Lett. 83 (2003) 2895.
[9] M. Tanaka, J.P. Harbison, M.C. Park, Y.S. Park, T. Shin, G.M. Rothberg, Appl. Phys. Lett. 65 (1994) 1964.
[10] Y. Morishita, K. Iida, J. Abe, K. Sato, Jpn. J. Appl. Phys. Part 2 36 (1997) L1100.
[11] L. Däweritz, M. Kästner, T. Hesjedal, T. Plake, B. Jenichen, K.H. Ploog, J. Cryst. Growth 251 (2003) 297.
[12] D. Kolovos-Vellianitis, C. Herrmann, L. Däweritz, K.H. Ploog, Appl. Phys. Lett. 87 (2005) 092505.
[13] L. Däweritz, F. Schippan, A. Trampert, M. Kästner, G. Behme, Z.M. Wang, M. Moreno, P. Schützendübe, K.H. Ploog, J. Cryst. Growth 227/228 (2001) 834.
[14] V.M. Kaganer, B. Jenichen, F. Schippan, W. Braun, L. Däweritz, K.H. Ploog, Phys. Rev. B 66 (2002) 045305.
[15] B.T.M. Willis, H.P. Rooksby, Proc. Phys. Soc. London B 67 (1954) 290.
[16] J.B. Goodenough, J.A. Kafalas, Phys. Rev. 157 (1967) 389.
[17] S. Haneda, N. Kazama, Y. Yamaguchi, H. Watanabe, J. Phys. Soc. Japan 42 (1977) 1201.
[18] A.M. Stoffel, J.W. Schneider, F.G. Hartmann, IEEE Trans. Magn. 6 (1970) 545.
[19] V.M. Kaganer, B. Jenichen, F. Schippan, W. Braun, L. Däweritz, K.H. Ploog, Phys. Rev. Lett. 85 (2000) 341.
[20] L. Däweritz, L. Wan, B. Jenichen, C. Herrmann, J. Mohanty, A. Trampert, K.H. Ploog, J. Appl. Phys. 56 (2004) 5056.
[21] Y. Takagaki, E. Wiebicke, L. Däweritz, K.H. Ploog, Appl. Phys. Lett. 85 (2004) 1505.
[22] R.C. Weast (Ed.), CRC Handbook of Chemistry and Physics, 62nd ed., CRC Press, Boca Raton, FL, 1981.
[23] J. Stephens, R.K. Kawakami, J. Berezovsky, M. Hanson, D.P. Shepherd, A.C. Gossard, D.D. Awschalom, Phys. Rev. B 68 (2003) 041307.

[24] J.J. Berry, S.J. Potashnik, S.H. Chun, K.C. Ku, P. Sciffer, N. Samarth, Phys. Rev. B 64 (2001) 052408.
[25] Y. Takagaki, E. Wiebicke, J. Mohanty, T. Hesjedal, L. Däweritz, K.H. Ploog, Physica E 24 (2004) 115.
[26] The selectivity between α- and β-MnAs in the wet chemical etching was falsely stated in: Y. Takagaki, E. Wiebicke, M. Ramsteiner, L. Däweritz, K.H. Ploog, Appl. Phys. A 76 (2003) 837, as we had failed to notice the conversion from the β phase to the α phase in narrow channels due to a partial stress release described in: Y. Takagaki, E. Wiebicke, T. Hesjedal, H. Kostial, C. Herrmann, L. Däweritz, K.H. Ploog, Appl. Phys. Lett. 83 (2003) 2895.
[27] H. Morinaga, M. Suyama, M. Nose, S. Verhaverbeke, T. Ohmi, IEICE Trans. Electron. E79-C (1996) 343.
[28] H. Morinaga, T. Hoshino, Y. Omura, M. Kitagawa, M. Aoki, Electrochemical Society Proceedings, vol. 99–36, 2000.
[29] D.W. Oscarson, P.M. Huang, C. Defosse, A. Herbillon, Nature 291 (1981) 50.
[30] Y. Takagaki, B. Jenichen, C. Herrmann, E. Wiebicke, L. Däweritz, K.H. Ploog, Phys. Rev. B, in press.
[31] G. Fischer, W.B. Pearson, Can. J. Phys. 36 (1958) 1010.
[32] K. Bärner, Phys. Lett. 35A (1971) 333.
[33] K. Bärner, Phys. Stat. Sol. (B) 84 (1977) 385.
[34] U. Neitzel, K. Barner, J. Phys. C 11 (1978) 4975.
[35] A. Erle, K. Bärner, J. Magn. Magn. Mater. 74 (1988) 225.
[36] K. Hirakawa, S. Katsumoto, T. Hayashi, Y. Hashimoto, Y. Iye, Phys. Rev. B 65 (2002) 193312.
[37] N. Kawamiya, Y. Nishino, M. Matsuo, S. Asano, Phys. Rev. B 44 (1991) 12406.
[38] Y. Nishino, S. Inoue, S. Asano, N. Kawamiya, Phys. Rev. B 48 (1993) 13607.
[39] Y. Nishino, M. Kato, S. Asano, K. Soda, M. Hayasaki, U. Mizutani, Phys. Rev. Lett. 79 (1997) 1909.
[40] A.M. Grishin, S.I. Khartsev, K.V. Rao, Appl. Phys. Lett. 68 (1996) 2008.
[41] E. Fawcett, Rev. Mod. Phys. 60 (1988) 209.
[42] E. Fawcett, H.L. Alberts, V.Y. Galkin, D.R. Noakes, J.V. Yakhmi, Rev. Mod. Phys. 66 (1994) 25.
[43] M.K. Niranjan, B.R. Sahu, L. Kleinman, Phys. Rev. B 70 (2004) 180406.
[44] H. Yamaguchi, A.K. Das, A. Ney, T. Hesjedal, C. Pampuch, D.M. Schaadt, R. Koch, Europhys. Lett. 72 (2005) 479.
[45] R.H. Wilson, J.S. Kasper, Acta Crystallogr. 17 (1964) 95.
[46] G.E. Bacon, R. Street, Nature (London) 175 (1955) 518.